Journal Pre-proof

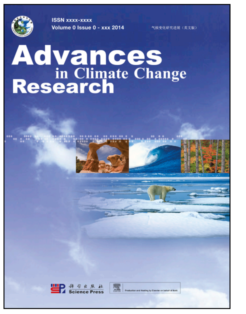

Testing and modeling of frozen clay–concrete interface behavior based on large-scale shear tests

He Peng-Fei, Mu Yan-Hu, Ma Wei, Huang Yong-Ting, Dong Jian-Hua

PII: S1674-9278(20)30073-3

DOI: https://doi.org/10.1016/j.accre.2020.09.010

Reference: ACCRE 201

To appear in: *Advances in Climate Change Research*

Received Date: 20 January 2020

Revised Date: 3 September 2020

Accepted Date: 30 September 2020

Testing and modeling of frozen clay–concrete interface behavior based on large-scale shear tests

HE Peng-Fei [1,2,3,4], MU Yan-Hu [1], MA Wei [1,3*], HUANG Yong-Ting [1,3], DONG Jian-Hua [4]

1. State Key Laboratory of Frozen Soil Engineering, Northwest Institute of Eco-Environment and Resources, Chinese Academy of Sciences, Lanzhou, 730000, China;

2. School of Science, Lanzhou University of Technology, Lanzhou, 730050, China;

3. University of Chinese Academy of Sciences, Beijing, 100049, China;

4. Key Laboratory of Disaster Prevention and Mitigation in Civil Engineering of Gansu Province, Lanzhou University of Technology, Lanzhou, 730050, China;

** Corresponding author: Ma W., Email: mawei@lzb.ac.cn, State Key Laboratory of Frozen Soil Engineering, Chinese Academy of Sciences, Lanzhou, 730000, China;*

Abstract

The shear behavior of the frozen soil–structure interface is important for accurately predicting the interface responses of structures adopted in the cold regions. The purpose of this study is to experimentally and theoretically investigate the shear behavior of frozen clay–concrete interface under engineering conditions. A large-scale direct shear apparatus with a temperature-controlled shear box is used to test the interface behavior. Test specimens consisting of a cement concrete block and frozen soil with initial water content ranging between 14.6% and 24.6% were prepared at different conditions of temperatures (15.4 to –9.8 °C), shear rates (0.03–0.9 mm min^{-1}), and normal stresses (50–200 kPa). It is found that the peak shear strength is linear developing with increasing of normal stress, initial water content, and temperature. It increased from 67.7 to 133.3 kPa as the initial water content increased from 14.9% to 24.6% at temperature of –6.8 to –6.6 °C, and it increased from 51.2 to 80.6 kPa with temperature decreasing from 15.4 to –9.8 °C at initial water content of 14.6% to 14.9%, furthermore it has a power law relationship with shear rate. The final vertical displacement increases with the decreasing temperature, and increasing initial water content. While, it is slight or could be ignored at lower shear rates (e.g. 0.03 mm min^{-1} and 0.15 mm min^{-1}) and it is –0.25 mm and –0.28 mm at shear rate of 0.3 mm min^{-1} and 0.9 mm min^{-1}, respectively. In addition, the evolution of vertical displacement also varies with test condition, the growth rate at beginning increases with increasing initial water content and decreasing temperature or ice content, which is because of the ice film effects the particle size. Moreover, a disturbed state concept model combined with linear and nonlinear characteristics is developed to describe the interface shear behavior. The disturbance *D* reflects the interface mechanical response and responds differently trend for different test conditions, increasing faster with increasing temperature and decreasing initial water content or shear rate. The testing results, including the test and model results, can be used to simulate the performance of engineered geotechnical assets such as earth dams or irrigation channels with concrete linings in cold regions.

Keywords: Shear strength; Frozen clay-concrete interface; Disturbed state concept; Constitutive model

1 Introduction

Cold regions in which permafrost and seasonal frozen ground extensively exist have experienced remarkable increases in population and expansion of infrastructure such as civil facilities, industrial projects, roads, and hydraulic and energy engineering projects. The heat balance of the ground will be changed not only by the surface pavement (including changes in water content and soil properties) but also by global warming (Jin et al., 2000, 2008; Wu et al., 2002). Especially in the permafrost regions, the increasing temperature due to human activity leads to a serious permafrost degradation and thermal hazard, which manifests as ice melting, water migration, and soil structure reconstruction (Wu and Zhang, 2008; Mu et al., 2014). Moreover, it has significantly adverse impact on the stability of engineering infrastructure, which is primarily built in or on the frozen ground, because the mechanical properties of frozen soil are significantly affected by temperature and moisture content which will be changed during permafrost degradation (Lai et al., 2012; Zhou et al., 2016, 2018, 2020). For example, the increase in temperature reduces the carrying capacity and induces the embankment settlement. The contact force between irrigation canal linings, road or building piles with frozen soil is inevitably affected by the soil temperature and moisture content.

The shear resistance between structures and soils is one of the most important factors to affect engineering stability. In cold regions, the adhesion of ice at the structure interface changes the shear resistance once the weather is below freezing, and the maximum shear resistance is called the adfreeze strength (Parameswaran, 1978). The cementing strength directly affects the tangential frost heave force at the soil–structure interface that may cause to some unexpected damage to the structure, especially lining structures that, have damageable sheets. For example, the lining of an irrigation canal may experience frost heaving and freezing forces acting on the lining, potentially leading to lining instability, which subsequently cracks or breaks. Thereafter, a large amount of water can leak through the canal–lining gap leading to low conveyance efficiency and more serious damage. In actuality, grievous and widespread damage was reported to occur in concrete linings in Heilongjiang province (Sun et al., 1998; Li et al., 2014), the Qinghai–Tibet Plateau (Tian et al., 2019), and the Xinjiang Uygur Autonomous Region (Qin et al., 2019), in China and in other structures in cold regions (Sadzevicius et al., 2013). Therefore, various studies on the freeze strength have been performed.

Peener and Irwin (1969) performed a field test for the freeze strength between Leda clay and a steel pipe interface, and the results showed that the freeze strength rapidly declined during warming periods, although the temperature of soil remained below freezing point. Bondarenko and Sadovskii (1975) argued that temperature primarily affected interface cohesion rather than interface friction angle. Parameswaran (1979, 1981, 1987) conducted a series of pull-out tests to investigate the freeze strength between structural piles and sand or ice interfaces. The results showed that the freeze strength increased with increasing of loading rate and the development features of freeze strength followed a power law. Moreover, the freeze bond strength at the interface had two components, adhesion of the ice to the pile and soil grain friction at the pile–soil interface. Weaver and Morgenstern (1981) highlighted that the freeze strength of the pile interface was linearly correlated to the strength of the surrounding soil. According to Biggar and Sego (1993a, 1993b), soil salinity dramatically reduced the adfreeze bond strength even at low salinity values. Ladanyi (1995) and Kim et al. (2015) summarized that freeze bonds essentially depended on the physical properties of the soil, the characteristics of the interface, the temperature, and the type and rate of loading. Wang et al. (2019) evaluated the shear strength of a soil–steel plate under an improved roughness algorithm and found that the cohesive force and friction angle demonstrated a linear improvement with increasing surface roughness.

Two methods have been commonly used to investigate the interface shear strength between geomaterials: pull-out test and direct shear tests. The former usually determines the adfreeze bond strength at a pile and frozen soil interface (Terashima, 1997; Iospa et al., 2015). The latter is easier and more cost-effective to test the adfreeze strength between a plane structure and frozen soil interface (Lee et al., 2013; Wen et al., 2016; Aldaeef and Rayhani, 2017, 2018). To investigate the interface shear behavior more accurately, Zhao et al. (2013) designed a multi-functional direct shear system, which has a large-scale shear box with a contact area of 100×200 mm^2. Subsequently, several investigations performed tests to discuss the effects of temperature, surface roughness and boundary conditions on the adfreeze strength between a steel plate and frozen soil interface (Zhao et al., 2014, 2017; Shi et al., 2018). Liu et al. (2014) also developed a large-scale temperature-controlled direct shear apparatus with cuboid sample size $300 \times 300 \times 200$ mm^3.

An credible constitutive model for shear behavior is required for a numerical prediction of geotechnical engineering responses. The disturbed state concept (DSC) was initially introduced by Desai (1974) to study the behavior of over-consolidated soils. It is a simple, flexible, and general approach that like the damage model (Desai, 2016). The DSC has a mathematical framework not only for solids, but also for interfaces and joints between two materials. It has been successfully employed in numerical analysis of interfacial response. Desai et al. (1984) proposed a thin-layer element to simulate the shear behavior of the soil–structure interface, the thickness of which can be determined from laboratory tests. Seo et al. (2004) employed a combined model and DSC model to imitate the shear behavior between a geomembrane and geotextile, and the back-prediction results show good agreement with test results, especially for strain-softening behavior. Tougigh et al. (2014, 2016) utilized the DSC model, combining the hierarchical single surface to characterize the behavior of the interface between the fiber-reinforced polymer and soil, and the model was verified by laboratory testing results. Baghini et al. (2018) evaluated the softening behavior response of piles under axial uplift loading by the DSC model, and the results revealed a strong correlation between the model and field tests. Alyounis et al. (2019) studied the microstructural variation in the material, and combined the DSC model and critical disturbance to identify the initiation of liquefaction in saturated Ottawa sand–steel interfaces.

In summary, most existing investigations shown that the initial water content, temperature and surface stiffness had notable influences on interface strength, and most models are focused on the soil–structure interface in the unfrozen condition. The evolution of vertical displacement at different conditions is rare and unclear, but it is a very important parameter in the theoretical and numerical analysis. Accordingly, a series of large-scale direct shear tests were conducted in this study to investigate the shear behavior of the frozen clay–concrete interface. And, the influence of initial water content and temperature on the interface stress, deformation, strength and strength parameters were presented and analyzed. Then, a simple model was suggested to characterize the linear and nonlinear responses of frozen clay–concrete interface behavior based on the DSC model. The results of this research can be used to designing and simulating the behavior of engineered geotechnical structures such as pile foundation, retaining walls, and irrigation channels with concrete linings in the broad cold regions.

2 Experimental process

A large-scale temperature-controlled direct shear test system was used to collect data on the shear behavior of the frozen soil–concrete interface. This section describes the test soil and concrete block, interface preparation procedure, testing apparatus, and testing procedure.

2.1 Sample preparation

Soil used in this study was taken from a canal foundation of the Urumqi Water Supply Project, Xinjiang Uighur Autonomous Region, China. The grain size distribution obtained by the laser diffraction method (SAPRC, 2008) is shown in Fig. 1.

In the soil test procedure, all soils were naturally dried, fully stirred, crushed by roller, and then sifted through a sieve with 2 mm openings (No. 10). The basic physical properties of the soil were obtained according to the Chinese standard of soil test methods (SAMR, 2007, 2019) and included the specific gravity $G_s = 2.66$, liquid limit LL = 51.0%, plastic limit PL = 19.2%, plasticity index PI = 31.8%, maximum dry density $\rho_{d\text{-}max} = 1.73$ g cm^{-3}, optimum moisture content ω_{opt}=16.1%, and freezing point and super-cooling temperature of the saturated soil, which are −0.27 and −1.79 °C, respectively. This soil was classified as CH according to the unified soil classification system. After sieving, the soil was filled with distilled water to achieve a target initial water content (mass moisture content). Finally, it was fully mixed, sealed, and stored for 12 h at 20 °C to ensure uniform moisture distribution.

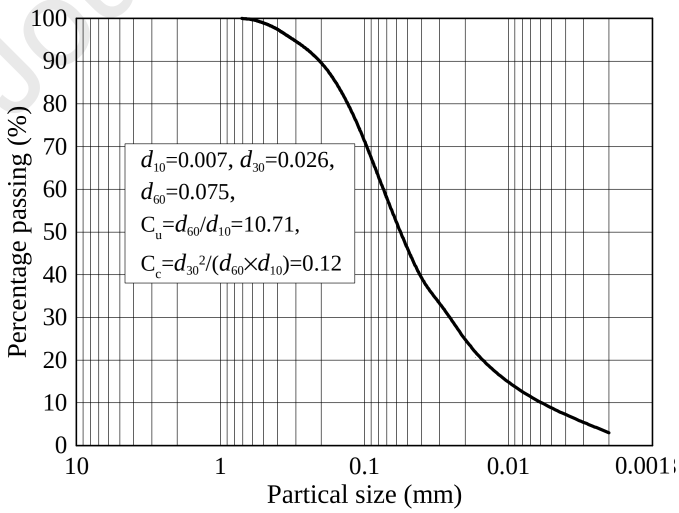

Fig. 1 Grain size distribution of test soil

The size of the concrete block was 300 mm × 300 mm × 100 mm (Fig. 2) and made from mortar consisting of ordinary Portland cement (Grade 32.5), natural river sand, and water by a mixing ratio of 1.8:3:1. The mortar was poured in a purpose-built box after mixed, and cured for 28 days (SAMR, 2010). The surface of the concrete block was smoothed during the preparation, and without any processing or damage after curing. So, the surface roughness detectable by the naked eye was smooth. It should be noted that the same concrete block was used in all tests and there was not obvious surface-damage after shearing, hence it is assumed that the surface roughness is constant throughout the tests.

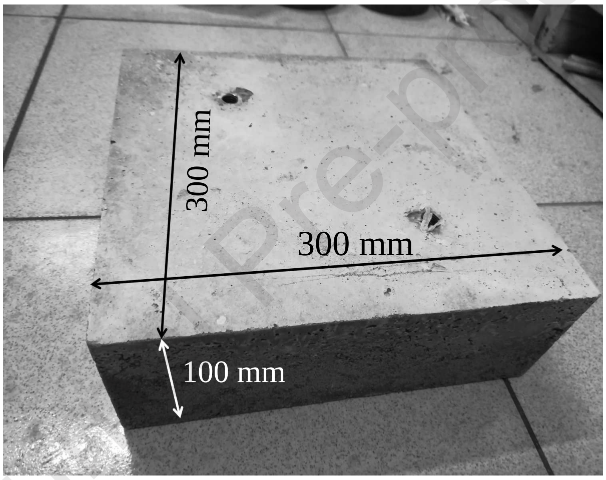

Fig. 2 The concrete block in the test.

2.2 Apparatus and testing procedure

A large-scale temperature-controlled direct shear apparatus (TZJ-150) in the Frozen Soil Laboratory at Beijing Jiaotong University was used to investigate the shear behavior of the frozen soil–concrete interface (Liu et al., 2014). A general view of the apparatus is shown Fig. 3. The normal force and horizontal force were imposed by two motors with maximum outputs of 100 kN and 150 kN, respectively. The normal and horizontal displacements were collected by two precise transducers, which were connected with a feedback control module to obtain precise control. The shear box was designed in two parts, the upper and lower shear boxes, with the same size of 300 mm × 300 mm × 100 mm. Two cooling path circulators were accommodated around the shear box and connected to two heating-cooling circulators, which could impose a temperature in the range of –20 °C to 60 °C. Additionally, the shear boxes were wrapped in a thermal insulating layer consisting of expanded polystyrene sheets to maintain temperature equilibrium. This system with good precision was introduced and used by Liu et al. (2014).

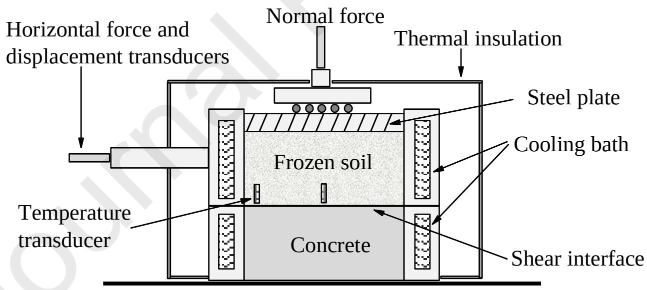

Fig. 3 Diagram of large-scale direct shear apparatus

To test the interface behavior between the frozen soil and concrete, the concrete block was fixed in the lower shear box first. Then, the wet soil with target initial water content was remolded on the concrete by compacting the soil in four layers using the vertical loading module. The dry density of compacted soil is 1.6 g cm^{-3}. After compacting soil in the first layer, two temperature transducers were installed near the shear interface (but not contacted with the concrete surface) to monitor the interface temperature. One transducer was installed in the middle and the other was near the edge. After compaction, a layer of plastic film was used to cover the soil to reduce moisture loss. The temperature of the sample was decreasing by using cooling bath circulation until reaching thermal equilibrium, usually more than 24 h. Once the temperature reached a target value and stabilized, the vertical force was set followed by a horizontal force, which pushed the upper shear box causing it to move at a certain shear rate. All of the testing data, including normal stress, vertical displacement, interface shear stress, and horizontal displacement, were automatically recorded by a computer. The recorded interface temperature was the average value of two temperature transducers. After shearing and thawing of the soil, three points near the interface were selected to obtain the average initial water content. Before the next test, the soil in the upper box was removed and the concrete interface was cleaned carefully. A total of thirteen effective tests were performed for different normal stresses, interface temperatures, initial water contents, and shear rates as shown in Table 1. The temperatures with differences of less than 1 °C and the initial water contents with differences of less than 1% were considered to be the same value for the analysis.

Table 1 Sample with different factors

Sample number (No.)	Normal stress (kPa)	Interface temperature (°C)	Initial water content (%)	Shear rate (mm min^{-1})
1	50	−6.6	14.9	0.30
2	100	−6.6	14.9	0.30
3	200	−6.3	14.8	0.30
4	100	−3.3	14.6	0.30
5	100	−9.8	14.9	0.30
6	100	−6.7	18.3	0.30
7	100	−6.8	24.6	0.30
8	100	−6.9	14.6	0.90
9	100	−6.3	15.1	0.15
10	100	−6.1	14.7	0.03
11	50	15.2	14.9	0.30

12	100	15.4	14.9	0.30
13	200	15.2	14.9	0.30

3 Experimental results and discussion

The results of the tests at different normal stress states are shown in Fig. 4. As can be seen in Fig. 4a, the interface experienced a strain-hardening behavior with ductile failure both in frozen and unfrozen interfaces such that shear stress initially increased quickly with increasing horizontal displacement and then grew slowly until reaching a steady value. At a given normal stress, the shear stress at the frozen interface was larger than that at the unfrozen interface due to ice strength at increasing of the interface adhesion force between frozen soil and concrete (Aldaeef and Rayhani, 2014; Liu et al., 2014; Wen et al., 2016). Fig. 4b shows the vertical displacement vs. horizontal displacement, where negative displacements indicate dilation of the shear band. For the frozen interface, an obvious dilation from beginning to the end of shearing process was seen at 50 and 100 kPa, while a plain followed by a dilating phase was revealed at 200 kPa owing to the higher normal stress restrained soil particles rolling (Alias, 2014). For the test of the unfrozen interface, under 50 and 100 kPa of normal stress, the soil volume tended to dilate while it contracted slightly at 200 kPa. It also can be seen that the vertical displacement under freezing condition was greater than that under melting condition because the frozen moisture films around soil particles, which increased in size, resulting in the change of effective particle contact area and load distribution mechanism of contact (Islam et al., 2011). The shear strength envelope in normal stress-shear stress plane is shown in Fig. 4c. It is noted that the shear strength is selected corresponding to 3 mm of horizontal displacement for the strain-hardening behavior or the peak stress for the strain-softening behavior (Andersland and Anderson, 1978). It can be seen in Fig. 4c that the shear strength and the normal stress are well correlated with a linear fitting function. As in the case of frozen interface, the interface friction angle was 27.8° and the interface cohesion was 15.1 kPa. At the unfrozen interface, the interface friction angle was 19.8° and the interface cohesion was 13.3 kPa. This is likely due to the ice crystals enhancing the interlocking force with soil particles resulting in a higher internal friction angle of soil and interface friction resistance between frozen soil and structures (Aldaeef and Rayhani, 2018).

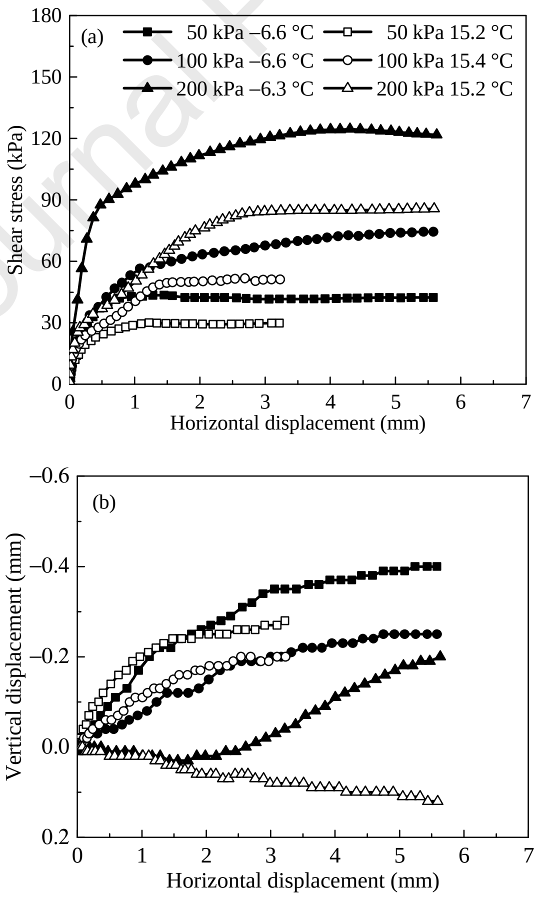

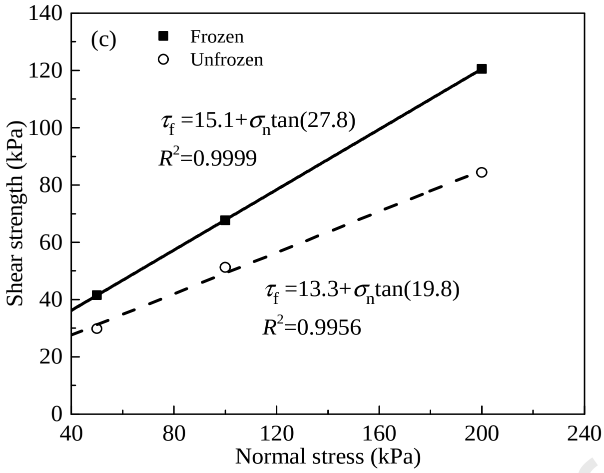

Fig. 4 Experimental results at frozen (–6.6 to –6.3 °C) and unfrozen (15.2–15.4 °C) conditions under different normal stresses, (a) shear stress versus horizontal displacement, (b) vertical displacement versus horizontal displacement, and (c) shear strength envelope.

The effect of temperature on the interface behavior is exhibited in Fig. 5. The evolution of the mobilized shear stress with horizontal displacement imposed shows that (Fig. 5a), the shear stress behavior at −3.3 °C was similar to that at 15.4 °C, and the initial stiffness increased with decreasing of temperature. The failure modes changed from strain-hardening to strain-softening as the temperature decreased from 15.4 °C to −9.8 °C due to the increasing ice content with decreasing temperature, and ice is a brittle failure material. These results agreed with previous studies of Wen et al. (2014), Zhao et al. (2014), and Liu et al (2014). Fig. 5b shows the interface vertical displacement with respect to the horizontal displacement, and testing result indicates that the interface tended to dilate from the beginning to the end during the test and the value increased slightly with decreasing of temperature because of increasing particle size with decreasing of temperature, as mentioned earlier. The interface shear strength vs. test temperature is shown in Fig. 5c, where the interface shear strength increased from 51.2 to 80.6 kPa with test temperature decreasing from 15.4 °C to −9.8 °C. In contrast, the interface shear strength does not change significantly when the temperature is above 0 °C (Andersland and Anderson, 1978). Therefore, the interface shear strength at 15.4 °C was taken as the shear strength at 0 °C, and had a linear fit for shear strength and temperature:

$$\tau_f = -3.1\,T + 48.1 \quad (1)$$

where τ_f is the shear strength (kPa) and T is the temperature (°C); R^2 was found to be 0.93845. This result was agreed well with the studies reported by Crory (1966) for the temperature in the range of −4 to 0 °C, Liu et al. (2014) for the temperature in the range of −16 to 0°C, and Aldaeef and Rayhani (2017) for temperature between −10 to −1°C .

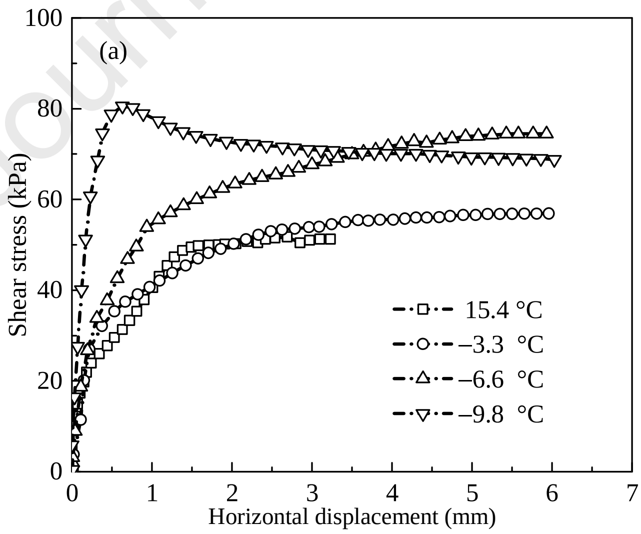

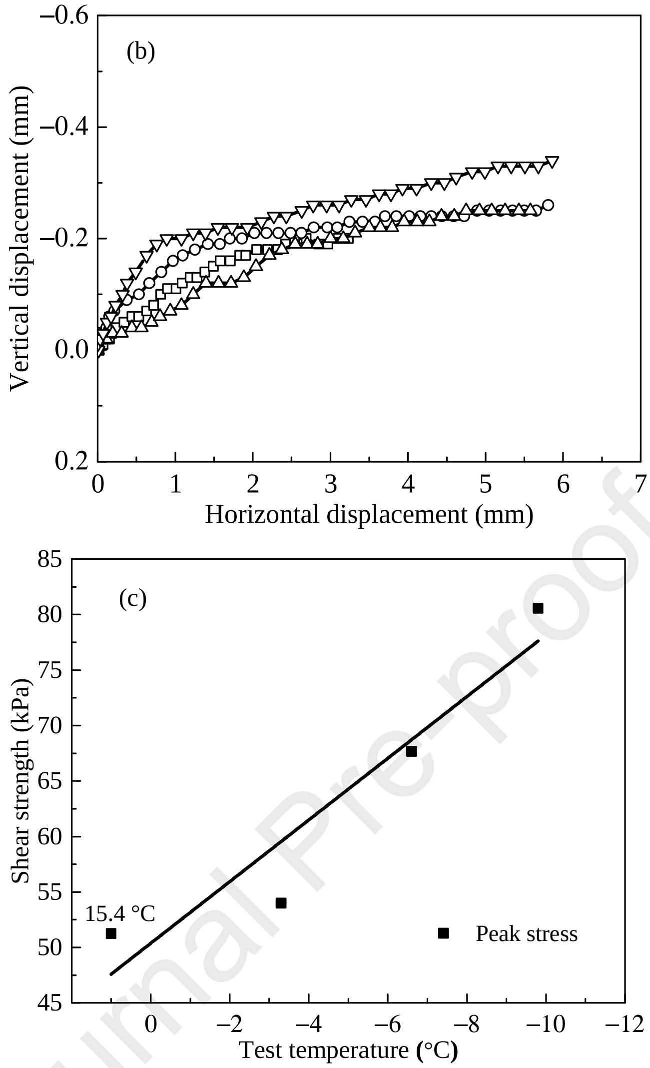

Fig. 5 Experimental results at different test temperatures under shear rate of 0.3 mm min^{-1}, normal stress of 100 kPa and initial water content of 14.6%–14.9%, (a) shear stress versus horizontal displacement, (b) vertical displacement versus horizontal displacement, and (c) shear strength versus test temperature

Experimental results of different initial water contents are displayed in Fig. 6. Similar results with strain-hardening behavior of the interface were obtained at initial water contents of 14.9% and 18.3% in Fig. 6a, while a pronounced strain-softening behavior was seen at the initial water content of 24.6% due to the elevated ice content at the interface with increasing initial water content and decreasing temperature

(Parameswaran, 1981, 1987; Liu et al., 2014; Wang et al., 2019). Additionally, the frozen soil is a fragile material in a state of lower temperature and higher initial water content (Cory, 1966). The variation in vertical displacement with the horizontal displacement is plotted in Fig. 6b. The interface dilated slowly during the test at the initial water contents of 14.9% and 18.3%. As in the case of 24.6%, the interface initially dilated significantly followed by moderate growth in which the shear stress exceeded the maximum. This might contribute to the increased adhesion force and the particle size including soils, ice crystals, and combinations of them due to the increase in initial water content. The interface shear strength increased from 67.7 to 133.3 kPa as the initial water content increased from 14.9% to 24.6% (Fig. 6c).

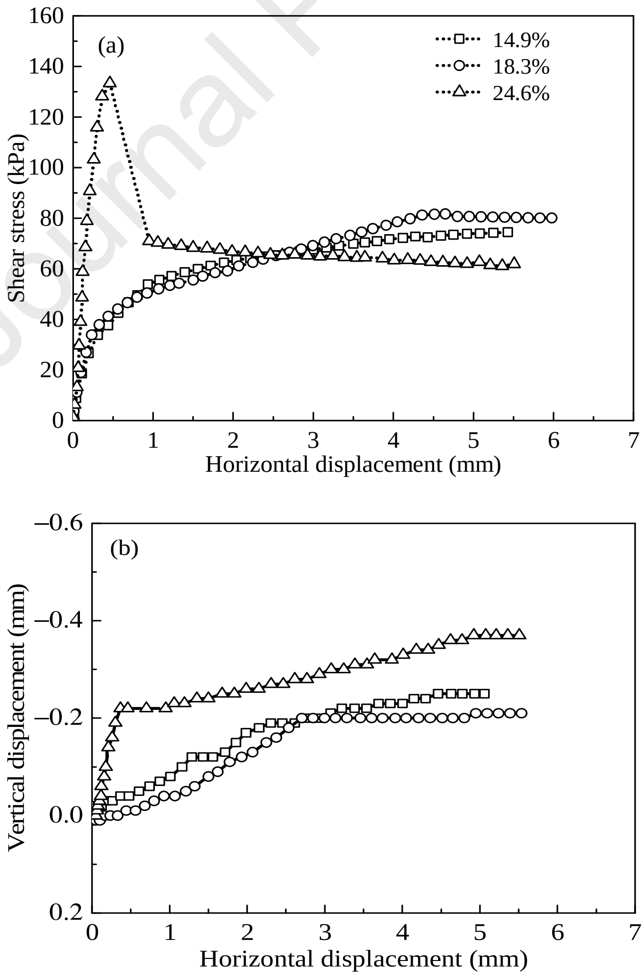

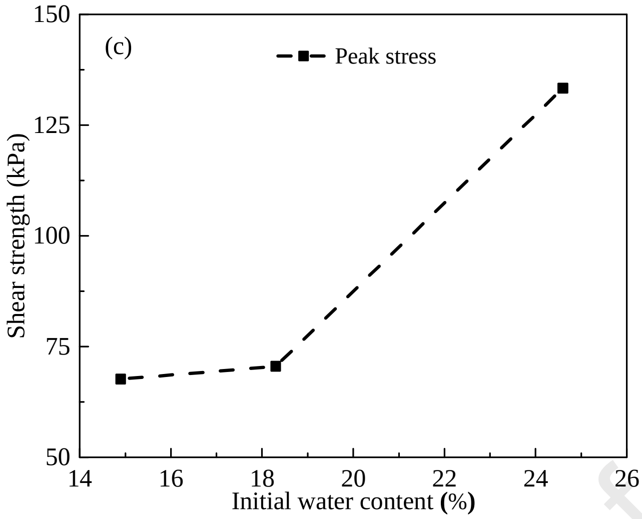

Fig. 6 Experimental results at different initial water contents under shear rate of 0.3 mm min^{-1}, normal stress of 100 kPa, and –6.8 °C to –6.6 °C, (a) shear stress versus horizontal displacement, (b) vertical displacement versus horizontal displacement, and (c) shear strength versus initial water content.

Results for four shear rates are presented in Fig. 7, indicating that similar strain-hardening behavior of the interface was obtained in all cases (Fig. 7a). The change of the volume could be neglectable at the shear rate of 0.03 and 0.15 mm min^{-1} (Fig. 7b), which was probably due to soil particles sliding or dragging along the interface, as well as inhibited particle-rolling at a lower rate (Xiu et al., 2019). The volumetric dilation of the interface was slightly during the test (Fig. 7b) at shear rate of 0.3 and 0.9 mm min^{-1}. Interface shear strength vs. shear rate is shown in Fig. 8c. Results show that the interface shear strength increased obviously as shear rate increased from 0.03 to 0.3 mm min^{-1}, and it increased slowly when the shear rate exceeded 0.3 mm min^{-1}. This behavior can be explained because at higher shearing rates, less time is allowed for rearrangement of particles at the interface (Einav and Randolph, 2006; Lefebvre and Leboeuf, 1987). These results agreed with a simplified method proposed by Parameswaran (1978) for the determination of long-term strength, where the interface shear strength and shear rate have a power law relationship as follows:

$$\tau_\mathrm{f} = 69.88 v^{0.44} \tag{2}$$

where τ_f is the interface shear strength, and v is the shear rate. The correlation coefficient R^2 was found to be 0.91439 (Fig. 7c).

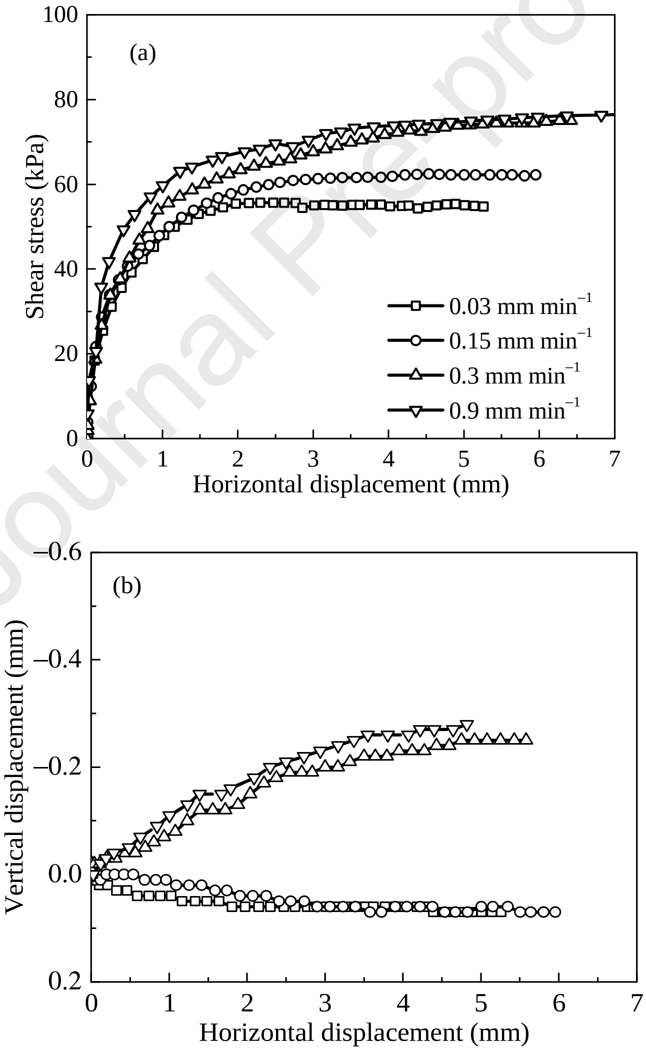

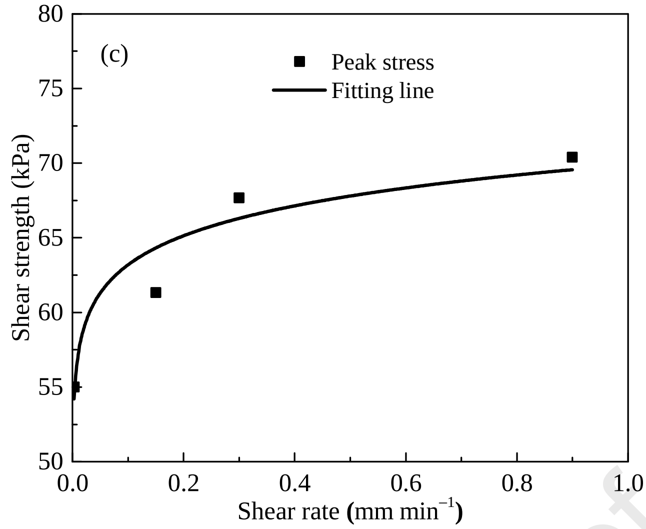

Fig. 7 Experimental results at different shear rates under normal stress of 100 kPa, initial water content of 14.6%–14.9%, and temperature of −6.9 to −6.1 °C, (a) shear stress versus horizontal displacement, (b) vertical displacement versus horizontal displacement, and (c) shear strength versus shear rate.

4 Constitutive modeling

The disturbed state concept (DSC) is established on a transparent theory that any and all stages during the deformation of a material are the mixture of materials in two stages called relative intact (RI) and fully adjusted (FA) (Desai, 2016). The former is defined the response of continuum materials and the latter is defined as the approximation of the ultimate asymptotic response of the materials. Disturbances that are caused by micro-cracking and softening (or stiffening due to external loads) can continually transform the initial RI state of materials to the FA state until all of the materials are in the critical state (Seo et al., 2004). The disturbance, as denoted by parameter *D*, represents the differences between the RI and the observed behavior or differences between the FA and the observed behavior (Desai, 2016). Fig. 8 shows a typical relationship between RI (r), observed behavior (a), and FA (c). It appears that the observed behavior of materials is represented by D, which is coupled with the RI state and FA state. Therefore, the crucial factor of DCS is the disturbance function D, which models the holistic behavior of the interaction mechanism in clusters of RI and FA states, rather than on the particle level processes (Al-Mhaidib, 2005; Kwak et al., 2013). The RI state can be defined using continuum models such as elastic or plastic models, and the FA state also can be defined using elastic, plastic, or pore models (Desai, 2016).

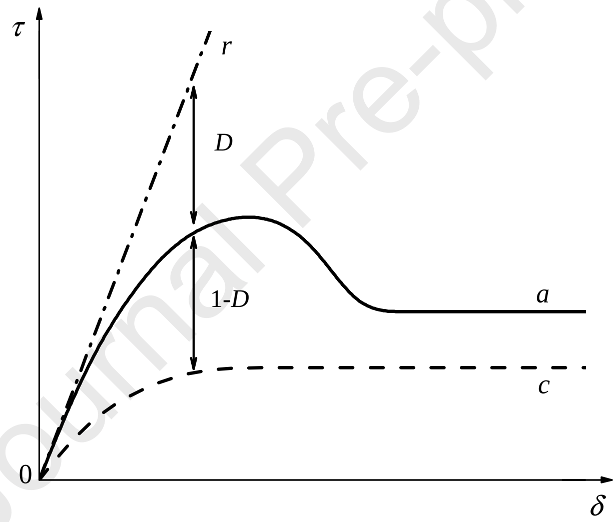

Fig. 8 Schematic of shear stress-horizontal displacement behavior in DSC theory.

Based on the DCS theory, the equilibrium of forces in the observed, RI and FA states, for a material element is derived as (Kwak et al., 2013)

$$\sigma_{ij}^{a} = (1-D)\sigma_{ij}^{r} + D\sigma_{ij}^{c} \tag{3}$$

where σ_{ij} is the stress tensor; the superscripts a, r, and c denote observed, RI, and FA states of the material, respectively; and D is the disturbance function. The behavior of materials is in a perfect RI state when D = 0, and it is in a perfect FA state when D = 1 (Desai, 2000). This formula appears to be similar to damage theory, but the element is different (Desai, 2016). Eq. (3) can be expressed as an incremental equation:

$$\mathrm{d}\sigma_{ij}^{a} = (1-D)\mathrm{d}\sigma_{ij}^{r} + D\mathrm{d}\sigma_{ij}^{c} + \mathrm{d}D\left(\sigma_{ij}^{c} - \sigma_{ij}^{r}\right) \tag{4a}$$

or

$$\mathrm{d}\sigma_{ij}^{a} = (1-D)C_{ijkl}^{r}\mathrm{d}\varepsilon_{kl}^{r} + DC_{ijkl}^{c}\mathrm{d}\varepsilon_{kl}^{c} + \mathrm{d}D\left(\sigma_{ij}^{c} - \sigma_{ij}^{r}\right) \tag{4b}$$

where d denoted the increment and, C_{ijkl} is the constitutive tensor.

For interface shear behavior, only the shear stress at the shear direction is considered and the other stress components are ignored; therefore, Eq. (3) can be simplified as

$$\tau^{a} = (1-D)\tau^{r} + D\tau^{c} \tag{5}$$

where τ is the shear stress.

4.1 Relative intact (RI) state

As mentioned previously, the response of the interface in the RI state can be represented by an elastic or elastic-plastic model. The interface shear behavior between frozen soil and concrete features elasticity at the initial deformation or uninjured status (Park and Desai, 2000; Lee et al., 2013; Liu et al., 2014). Hence, a reasonable assumption is that the interface has linear elastic behavior in the RI state and ignores the effect of volume change on horizontal deformation. The interface obeys Hooke's law, which can be represented as (Kwak et al., 2013)

$$\tau^{r} = K_{o}\delta \tag{6}$$

where K_{o} is the original stiffness of interface shear behavior, and δ is the horizontal displacement.

4.2 Fully adjusted (FA) state

As a simple approach, it is assumed that the interface with the FA state still has some strength from friction resistance with an impairing cohesion (Bondarenko and Sadovskii, 1975; Ladanyi, 1995; Zhao et al., 2017; Shi et al., 2018). The hyperbolic model is a simple, classic, and wide model applied to simulate the response of geomaterials and interface behavior (Al-Shayea et al., 2003; He et al., 2018). Accordingly, the response of the interface can be described as (Cao et al., 2013)

$$\tau^c = \frac{\delta}{\alpha + \beta\delta} \tag{7}$$

where α and β are the parameters of the model.

4.3 Disturbance function

The disturbance function D is defined based on the experimental and model results from the direct shear test and the above model, as follows (Desai, 2016; Kwak et al., 2013):

$$D = \frac{\tau^r - \tau^a}{\tau^r - \tau^c} \tag{8}$$

where the superscripts r, c, and a denote the RI, FA, and observed states, respectively.

The mathematical expression of D can be expressed using the Weibull function in terms of accumulated plastic displacements (Desai, 2016; Kwak et al., 2013):

$$D = D_{\mathrm{u}}\left[1 - \exp\left(-A\delta_{\mathrm{p}}^{z}\right)\right] \tag{9}$$

where D_{u} is the disturbed function value when the materials are in a fully disturbed state, A and Z are the parameters, and δ_{P} is a plastic displacement trajectory that refers to the summation of plastic deformation to the observed responses. Theoretically, D varies from 0.0 to 1.0, but many materials fail before reaching 1.0 (Desai, 2000). The plastic displacement trajectory can be calculated by

$$\delta_{\mathrm{p}} = \delta - \delta_{\mathrm{e}} \tag{10}$$

where δ_{e} is elastic deformation of the interface.

4.4 Parameters calculation

As indicated previously, the RI state is simulated using linear elastic behavior. In this case, the original stiffness (K_{o}) is calculated from the interface in the linear elasticity regime of shear deformation. The parameters in the FA state are calculated based on the test results. It is noted that the parameters from the test of No. 4 are selected to simulate the FA state under the normal stress of 100 kPa to obtain an effective comparison of D. The parameters A and Z can be calculated by taking the logarithm twice for the both sides of Eq. (9).

$$Z\ln\left(\delta_{\mathrm{p}}\right) + \ln\left(A\right) = \ln\left[-\ln\left(\frac{D_{\mathrm{u}} - D}{D_{\mathrm{u}}}\right)\right] \tag{11}$$

In the plot of δ_{p} vs. $\ln(-\ln((D_{\mathrm{u}}-D)/D))$, the parameters A and Z can be determined, and are listed in Table 2. The results indicate that K_{o} increased with the increasing of normal stress, temperature, and displacement rate, respectively.

Table 2 Model parameters

Sample Number (No.)	Relatively intact	Fully adjusted		Disturbance		
	K_{o} (kPa mm^{-1})	α (mm (kPa)$^{-1}$)	β (1 (kPa)$^{-1}$)	A	Z	D_{u}
1	132.6	0.0046	0.0310	2.29	0.42	1.0
2	176.5	0.0065	0.0170	3.16	0.20	1.0
3	317.7	0.0085	0.0094	2.11	0.48	1.0
4	125.0	0.0065	0.0170	11.69	0.88	1.0
5	356.7	0.0065	0.0170	2.20	0.48	1.0
6	156.9	0.0065	0.0170	2.10	0.29	1.0
7	419.8	0.0065	0.0170	2.80	0.90	1.0
8	189.7	0.0065	0.0170	2.46	0.50	1.0

9	160.2	0.0065	0.0170	4.51	0.64	1.0
10	134.5	0.0065	0.0170	4.72	0.56	1.0

The values of disturbance *D*, related to the plastic displacement trajectory δ_p from all direct shear test results are expressed in Fig. 9. The *D* vs. δ_p relationship shows a diverse trend for different test conditions and presents the interface response under loading. Fig. 9a shows that the increasing rate of *D* at 100 kPa was faster than that at 50 and 200 kPa, which indicates that the interface was more vulnerable to damage at 100 kPa at a certain δ_p. Fig. 9b shows the *D* vs. δ_p relationship at different temperatures, and it can be seen that the rate increased similar initially, and then the increasing rate of −9.8 °C was obviously lower than that of −6.6 and −3.3 °C. This indicates that the interface was less sensitive to damage at −9.8 °C than at −6.6 °C and −3.3 °C, which is due to the increased adhesive ice formed at the interface with the decreasing of temperature (Wang et al., 2019). Similar observations to those at different initial water contents can be seen in Fig. 9c where the increasing rate of *D* decreased with the higher initial water content. The effect of shear rates on the *D* vs. δ_p relationship is shown in Fig. 9d. *D* moved to the right with the increase in shear rate indicating that the interface is vulnerable at higher strain because that the instantaneous shear strength is greater than the long-term shear strength (Parameswaran, 1979; Ladanyi, 1995).

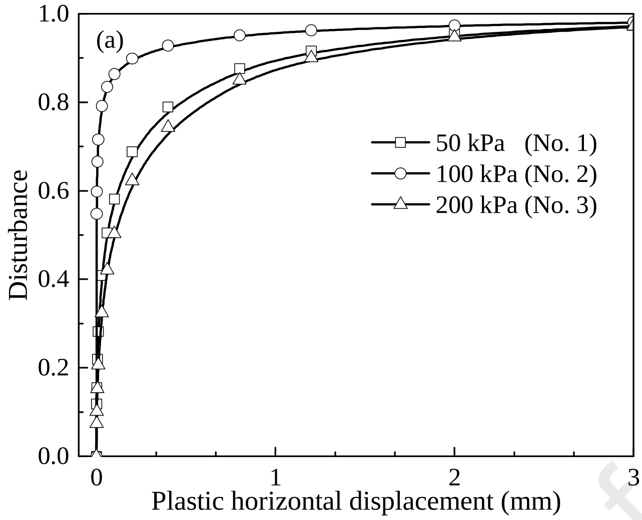
(a)
50 kPa (No. 1)
100 kPa (No. 2)
200 kPa (No. 3)
Disturbance
Plastic horizontal displacement (mm)
1.0
0.8
0.6
0.4
0.2
0.0
0
1
2
3

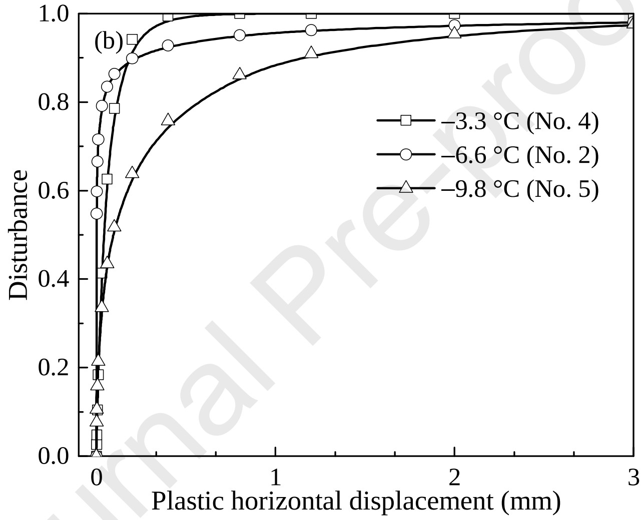
(b)
–3.3 °C (No. 4)
–6.6 °C (No. 2)
–9.8 °C (No. 5)
Disturbance
Plastic horizontal displacement (mm)
1.0
0.8
0.6
0.4
0.2
0.0
0
1
2
3

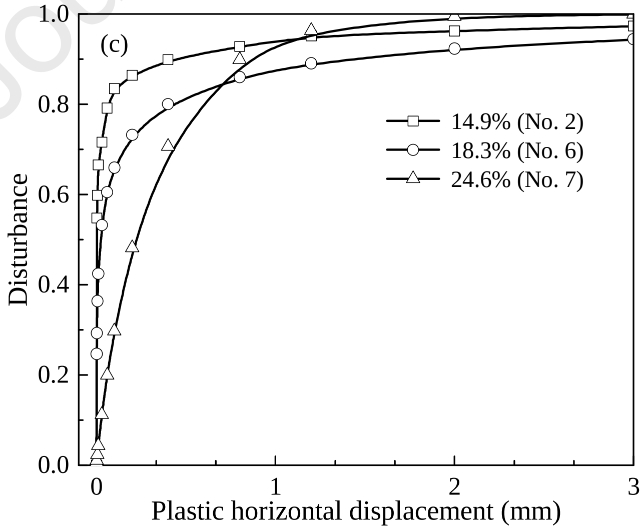
(c)
14.9% (No. 2)
18.3% (No. 6)
24.6% (No. 7)
Disturbance
Plastic horizontal displacement (mm)
1.0
0.8
0.6
0.4
0.2
0.0
0
1
2
3

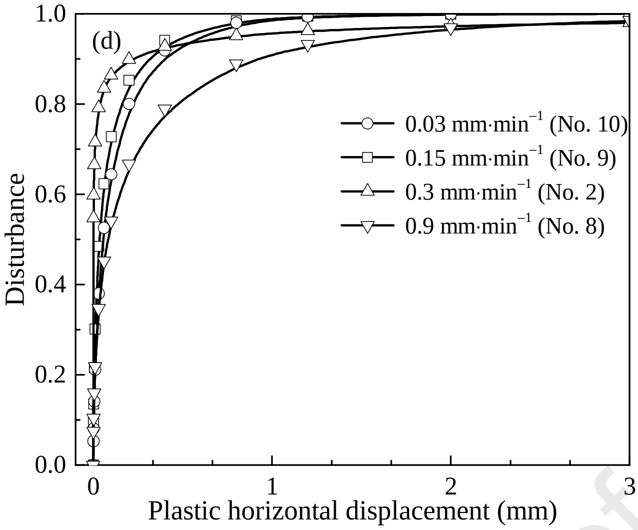

Fig. 9 Disturbance versus plastic horizontal displacement for different tests

4.5 Modeling results and discussion

The performance of the model was verified through the back-prediction using the incremental iterative method based on the direct shear test results for the interface. The incremental iterative equation can be obtained from Eq. (5), and is given by (Kwak et al., 2013).

$$\mathrm{d}\tau_{n+1}^{a} = \left(1 - D_{n+1}\right)\mathrm{d}\tau_{n+1}^{r} + D_{n+1}\mathrm{d}\tau_{n+1}^{c} + \mathrm{d}D_{n+1}\left(\sigma_{n}^{c} - \sigma_{n}^{r}\right) \tag{12a}$$

$$\mathrm{d}\tau_{n+1}^{r} = \tau_{n+1}^{r} - \tau_{n}^{r} \tag{12b}$$

$$\mathrm{d}\tau_{n+1}^{c} = \tau_{n+1}^{c} - \tau_{n}^{c} \tag{12c}$$

$$\mathrm{d}D_{n+1} = D_{n+1} + D_{n} \tag{12d}$$

where n is the step.

Figure 10 shows the comparison of observed and predicted results of the frozen soil–concrete interface using the DSC model. It can be seen that the predicted values were consistent with the test results, especially in the regions where the horizontal displacement was less than 3 mm for the strain-hardening behavior and the pre-peak regions for the strain-softening behavior. However, a slight discrepancy was found in regions with large horizontal displacement; the predicted values were smaller than the test values although the difference was minimal. The main reason is that the model enters a fully disturbed state when the disturbance *D* is 1, where the stress will change according to the hyperbolic model. But the testing result is till changing slightly due to the decreasing of contact are and others. So, there are some diversities between predicted and test value.

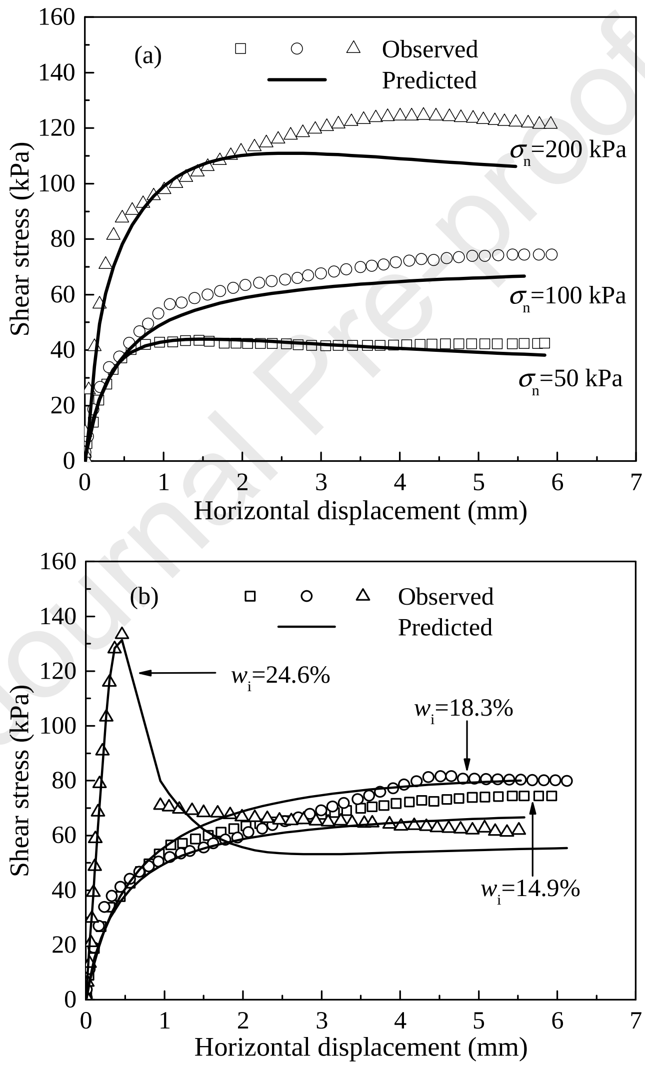

Fig. 10 Comparison between results of observed and predicted, (a) results of different normal stress, and (b) results of different initial water content.

5 Conclusions

Climate change and engineering activities can lead to permafrost degradation, especially the latter, which makes the permafrost degrading more pronounced. This results in an increase in the permafrost temperature, active layer thickness, and upper limit of permafrost. For the structures buried in the frozen soil, permafrost degradation changes the water content and temperature of the soil around the structure, then the physical and mechanical properties of these soil were varied, which in turn affects the engineering stability of structures including the interface stability between pile foundations, retaining walls, and irrigation channel lining with the soil. Hence, in this study, 13 sets of direct shear tests with different temperatures, initial water contents, shear rates, and normal stresses were performed to investigate the influence of permafrost degradation on the interface behavior between frozen clay and concrete. The disturbed state concept model was employed to describe the interface shear stress–horizontal displacement relationships. The test results and model parameters were analyzed and discussed, and the following conclusions can be drawn:

(1) The final vertical displacement was dilation for the frozen interface and lower normal stress of the unfrozen interface. It increases with the decreasing of temperature, and increasing of initial water content. While, it is slight or could be ignored at lower shear rates (e.g. 0.03 mm min^{-1} and 0.15 mm min^{-1}) and it is –0.25 mm and –0.28 mm at shear rate of 0.3 mm min^{-1} and 0.9 mm min^{-1}, respectively.

(2) For the normal stress of 100 kPa, the peak shear strength increased from 67.7

to 133.3 kPa as the initial water content increased from 14.9% to 24.6% at temperature of –6.8 to –6.6 °C, and it increased from 51.2 to 80.6 kPa with temperature decreasing from 15.4 to –9.8 °C at initial water content of 14.6% to 14.9%.

(3) The DCS model was applied to simulate the interface behavior between the frozen clay–concrete interface. It is easily applied to geotechnical engineering due to it combines linear and hyperbolic models. The predicted results were verified by the corresponding test results, although discrepancies coursed by tiny experimental control and parameter selection errors exist regarding the magnitude.

(4) The disturbance D reflects the interface response in loading process and shows a particular trend for different test conditions. It increased faster as temperature rose and initial water content, or shear rate decreased. D increased more rapidly indicating that the interface is more vulnerable to damage.

Acknowledgments

This work was supported by the Scientific Instrument Developing Project of the Chinese Academy of Science (YJKYYQ20180058), the National Natural Science Foundations of China (41772325), and the Scholarship for LUT Teachers' Overseas Studies, and Open Fund of National Key Laboratory of Frozen Soil Engineering (SKLFSE201603).

References

Aldaeef, A.A., Rayhani, M.T., 2017. Adfreeze strength and creep behavior of pile foundations in warming permafrost. 1st GeoMEast International Congress and Exhibition on Sustainable Civil Infrastructures: Innovative Infrastructure Geotechnology. Springer, Cham. pp.254–264.

Aldaeef, A.A., Rayhani, M.T., 2018. Influence of exposure temperature on shaft capacity of steel piles in ice-poor and ice-rich frozen soils. International Congress and Exhibition on Sustainable Civil Infrastructures: Innovative Infrastructure Geotechnology, Springer, Cham, pp.247–257.

Alias, R., Kasa, A., Taha M.R., 2014. Particle size effect on shear strength of granular materials in direct shear test. World Academy of Science, Engineering and Technology, International Journal of Civil, Environmental, Structural, Construction and Architectural Engineering. 8(11), 1144–1147.

Al-Mhaidib, A.I., 2005. Shearing rate effect on interfacial friction between sand and steel. The fifteenth International Offshore and Polar Engineering Conference, International Society of Offshore and Polar Engineers, pp.633–640

Al-Shayea, N., Abduljauwad, S., Bashir R., et al., 2003. Determination of parameters for a hyperbolic model of soils. P. I. Civil Eng-Geotec. 156(2), 105–117.

Alyounis, M.E., Desai, C.S., 2019. Testing and modeling of saturated interfaces with effect of surface roughness. II: modeling and validations. Int. J. Geomech. 19(8), 04019097.

Andersland, O., Anderson, D., 1978. Geotechnical engineering for cold regions.

McGraw-Hill College, New York.

Baghini, E.G., Toufigh, M.M., Toufigh, V., 2018. Analysis of pile foundations using natural element method with disturbed state concept. Comput. Geotech. 96, 178–188.

Biggar, K.W., Sego, D.C., 1993a. Field pile load tests in saline permafrost. I. test procedures and results. Can. Geotech. J. 30(1), 34–45.

Biggar, K.W., Sego, D.C., 1993b. Field pile load tests in saline permafrost. II. analysis of results. Can. Geotech. J. 30(1), 46–59.

Bondarenko, G.I., Sadovskii, A.V., 1975. Strength and deformability of frozen soil in contact with rock. Soil Mech. Found. Eng. 12(3), 174–178.

Cao, W., Chen, Y., Wolfe, W.E., 2013. New load transfer hyperbolic model for pile-soil interface and negative skin friction on single piles embedded in soft soils. Int. J. Geomech. 14(1), 92–100.

Crory, F.E., 1966. Pile foundations in permafrost. Proceedings of 1st Permafrost International Conference, Lafayette, Indiana, NAS-NRC Publ. 1287, pp. 467–472.

Desai. C.S., 1974. A consistent finite element technique for work-softening behavior. Proceedings of International Conference on Computer Mechanics, Methods in Nonlinear Mechanics, University of Texasat Austin, Austin, Texas.

Desai, C.S., 2000. Mechanics of Materials and Interfaces: The Disturbed State Concept. CRC press. Boca Raton, Florida.

Desai, C.S., 2016. Disturbed state concept as unified constitutive modeling approach.

J. Rock Mech. Geotech. Eng. 8(3), 277–293.

Desai, C.S., Zaman, M.M., Lightner, J.G., et al., 1984. Thin-layer element for interfaces and joints. Int. J. Num. Analy. Meth. Geomech. 8(1), 19–43.

Duncan, J.M., Chang, C.Y., 1970. Nonlinear analysis of stress and strain in soils. J. Soil Mech. Found. Div. 96(5), 1629–1653.

Einav, I., Randolph, M., 2006. Effect of strain rate on mobilised strength and thickness of curved shear bands. Géotechnique, 56(7), 501–504.

SAMR (State Administration for Market Regulation), 2007. GB/T50145-2007. Standard for Engineering Classification of Soil. China Planning Presss, Beijing (in Chinese).

SAMR (State Administration for Market Regulation), 2010. GB/T50082-2009Standard for Test Methods of Long-term Performance and Durability of Ordinary Concrete. China Architecture & Building Press, Beijing (in Chinese).

SAMR (State Administration for Market Regulation), 2019. GB/T50123-2019. Standard for Geotechnical Testing Method. China Planning Presss, Beijing (in Chinese).

SAPRC (Standardization Administration of the Peoples Republic of China), 2008. GB/T19077.1-2008. Particle size analysis: Laser diffraction method. Part 1: general principles. Beijing (in Chinese).

He, P.F., Ma, W., Mu, Y.H., et al., 2018. Study on freezing strength characteristics and formation mechanism of frozen soil-concrete interface. Trans. CSAE. 34

(23), 127–133 (in Chinese).

Iospa, A., Aksenov, V., Shmelev, I., 2015. Certain results of antiheave and anticorrosion tests of protective coatings for metal foundations on permafrost. Soil Mech. Found. Eng. 52(5), 277–281.

Islam, M.N., Siddika, A., Hossain, M.B., et al., 2011. Effect of particle size on the shear strength behavior of sands. Austral. Geomech. J. 46(3), 75–86.

Jin, H.J., Li, S., Cheng, G.D., et al., 2000. Permafrost and climatic change in China. Global Planet. Change, 26(4), 387–404.

Jin, H.J., Wei, Z., Wang, S., et al., 2008. Assessment of frozen-ground conditions for engineering geology along the Qinghai–Tibet highway and railway, China. Eng. Geol. 101(3-4), 96–109.

Kim, M., Seo, H., Lawson, W., et al., 2015. Tangential heave stress for the design of deep foundations revisited. 16th International Conference on Cold Regions Engineering, pp. 404–415.

Kwak, C.W., Park, I.J., Park, J.B., 2013. Evaluation of disturbance function for geosynthetic–soil interface considering chemical reactions based on cyclic direct shear tests. Soils Found. 53(5), 720–734.

Ladanyi, B., 1995. Frozen soil-structure interfaces. Stud. Appl. Mech. 42, 3–33.

Lai, Y.M., Xu, X.T., Dong, Y., et al., 2013. Present situation and prospect of mechanical research on frozen soils in China. Cold Reg. Sci. Tech. 87, 6-18.

Lee, J., Kim, Y., Choi, C., 2013. A study for adfreeze bond strength developed between weathered granite soils and aluminum plate. J. Korean. Geo. Soc.

14(12), 23–30.

Lefebvre, G., Leboeuf, D., 1987. Rate effects and cyclic loading of sensitive clays. J. Geotech. Eng. 113(5), 476–489.

Li, S.Y., Lai, Y.M., Pei, W.S., et al., 2014. Moisture-temperature changes and freeze-thaw hazards on a canal in seasonally frozen regions. Nat. Hazards, 72(2), 287–308.

Liu. J.K., Lv, P., Cui, Y., et al., 2014. Experimental study on direct shear behavior of frozen soil-concrete interface. Cold Reg. Sci. Technol. 104, 1–6.

Mu, Y.H., Ma, W., Niu, F.J., et al., 2014. Study on geotechnical harzards to roadway engineering in permafrost regions. J. Disaster Prev. Mitig. Eng. 34(3), 259-267 (in Chinese).

Perameswaran, V.R., 1978. Adfreeze strength of frozen sand to model piles. Can. Geotech. J. 15, 494–500.

Parameswaran, V.R., 1979. Creep of model piles in frozen soil. Can. Geotech. J. 16(1), 69–77.

Parameswaran, V.R., 1981. Adfreeze strength of model piles in ice. Can. Geotech. J. 18(1), 8–16.

Parameswaran, V.R., 1987. Adfreezing strength of ice to model piles. Can. Geotech. J. 24(3), 446–452.

Park, I.J., Desai, C.S., 2000. Cyclic behavior and liquefaction of sand using disturbed state concept. J. Geotech. Geoenviron. Eng. 126(9), 834–846.

Penner, E., Irwin, W.W., 1969. Adfreezing of Leda clay to anchored footing columns.

Can. Geotech. J. 6(3), 327–337.

Qin. Z., Lai. Y., Tian. Y., et al., 2019. Frost-heaving mechanical model for concrete face slabs of earthen dams in cold regions. Cold Reg. Sci. Tech. 161, 91–98.

Sadzevicius, R., Damulevicius, V., Skominas, R., 2013. The technical state of earth dams in Lithuania. J. Environ. Eng. Landsc. Manag. 21(3), 180–188.

Seo, M.W., Park, I.J., Park, J.B., 2004. Development of displacement-softening model for interface shear behavior between geosynthetics. Soil Found. 44(6), 27–38.

Shi, Q.B., Yang, P., Wang, G.L., 2018. Experimental research on adfreezing strengths at the interface between frozen fine sand and structures. Sci. Iranica. Tran. 25(2), 663–674.

Sun, J.M., Li, G.Y., Zhang, Q.Y., et al., 1998. Stability analysis of earth-rock dam slope on the action of ice cover. J. Heilongjiang Hydraul. Eng. Coll. 1, 26–28 (in Chinese).

Terashima, T., 1997. Comparative experiments on various adfreeze bond strength tests between ice and materials. WIT Trans. Eng. Sci. 14, 207–216.

Tian, Y.H., Yang, Z.H., Tai, B.W., et al., 2019. Damage and mitigation of railway embankment drainage trench in warm permafrost: a case study. Eng. Geol. 261, 105276.

Toufigh. V., Desai, C.S., Saadatmanesh, H., et al., 2014. Constitutive modeling and testing of interface between backfill soil and fiber-reinforced polymer. Int. J. Geomech. 14(3), 04014009.

Toufigh, V., Shirkhorshidi, S.M., Hosseinali, M., 2016. Experimental investigation and constitutive modeling of polymer concrete and sand interface. Int. J. Geomech. 17(1), 04016043.

Wang, T.L., Wang, H.H., Hu, T.F., et al., 2019. Experimental study on the mechanical properties of soil-structure interface under frozen conditions using an improved roughness algorithm. Cold Reg. Sci. Tech. 158, 62–68.

Weaver, J.S., Morgenstern, N.R., 1981. Pile design in permafrost. Can. Geotech. J. 18(3), 357–370.

Wen, Z., Yu, Q., Ma, W., et al., 2016. Experimental investigation on the effect of fiberglass reinforced plastic cover on adfreeze bond strength. Cold Reg. Sci. Technol. 131, 108–115.

Wu, Q.B., Zhang, T., 2018. Recent permafrost warming on the Qinghai-Tibetan Plateau. J. Geophys. Res. 113(D13).

Wu. Q.B., Liu, Y.Z., Zhang, J.M., et al., 2002. A review of recent frozen soil engineering in permafrost regions along Qinghai-Tibet Highway, China. Permafrost Periglac. 13(3), 199–205.

Xu, X., Li, Q., Xu, G., 2019. Investigation on the behavior of frozen silty clay subjected to monotonic and cyclic triaxial loading. Acta. Geotech. 1–14.

Zhao, L., Yang, P., Wang, J.G., et al., 2014. Cyclic direct shear behaviors of frozen soil–structure interface under constant normal stiffness condition. Cold Reg. Sci. Technol. 102, 52–62.

Zhao, L., Yang, P., Zhang, L.C., et al., 2017. Cyclic direct shear behaviors of an artificial frozen soil-structure interface under constant normal stress and sub-zero temperature. Cold Reg. Sci. Tech. 133, 70–81.

Zhao, L.Z., Yang, P., Wang, H.B., 2013. Development and application of large-scale multifunctional frozen soil–structure interface cycle-shearing system. Chin. J. Geotech. Eng. 35(4), 707–713 (in Chinese).

Zhou, Z.W., Ma, W., Zhang, S.J., et al., 2016. Multiaxial creep of frozen loess. Mech. Mater. 95, 172–191.

Zhou, Z.W., Ma, W., Zhang, S., et al., 2018. Effect of freeze-thaw cycles in mechanical behaviors of frozen loess. Cold Reg. Sci. Technol. 146, 9–18.

Zhou, Z.W., Ma, W., Zhang, S.J., et al., 2020. Experimental investigation of the path-dependent strength and deformation behaviors of frozen loess. Eng. Geol. 265, 105449.

Conflict of interest

The authors declare no conflict of interest.